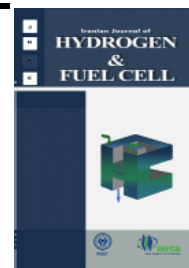


Iranian Journal of Hydrogen & Fuel Cell

IJHFC

Journal homepage://ijhfc.irost.ir



## Interaction of atomic hydrogen with monometallic Au(100), Cu(100), Pt(100) surfaces and surface of bimetallic Au@Cu(100), Au@Pt(100) overlayer systems: The role of magnetism

Razieh Habibpour \*, Eslam Kashi

Department of Chemical Technologies, Iranian Research Organization for Science and Technology, Tehran, Iran.

### Article Information

Article History:

Received:

07 Sep 2017

Received in revised form:

08 Dec 2017

Accepted:

11 Dec 2017

### Keywords

Hydrogen adsorption

Au (100)

Cu (100)

Pt (100)

DFT

### Abstract

The spin-polarized calculations in generalized gradient approximation density-functional theory (GGA-DFT) have been used to show how the existence of second metals can modify the atomic hydrogen adsorption on Au (100), Cu (100), and Pt (100) surfaces. The computed adsorption energies for the atomic hydrogen adsorbed at the surface coverage of 0.125 ML (monolayer) for monometallic Au (100), Cu (100), Pt (100) and bimetallic Au@Cu (100) and Au@Pt (100) surfaces are 3.98, 5.06, 4.13, 5.30, and 6.36 eV, respectively. Due to the adsorption of hydrogen atoms, the Au atoms of Au (100), Cu atoms of Cu (100), and Pt atoms of Au@Pt (100) surfaces tend to lose the  $6s^1$ ,  $4s^1$ , and  $6s^1$  electrons and reach the  $5d^{10}$ ,  $3d^{10}$ , and  $5d^9$  electronic configurations, respectively. In Pt (100), Au@Cu (100), and Au@Pt (100) systems, the spin-up and spin-down bands are asymmetric and shift significantly in opposite directions. Therefore, they are spin polarized; spin paramagnetism is also observed.

## 1. Introduction

An understanding of atomic hydrogen adsorption and its reaction with transition metal surfaces is

of fundamental interest. Its application in different areas is also interesting, e.g., the production of many chemicals and pharmaceuticals, surface etching in microelectronics, hydrogen storage

\*Corresponding Author's Fax: +982156276026

E-mail address: Habibpour@irost.ir

doi: 10.22104/ijhfc.2017.2455.1155

technologies, hydrogen generation, hydrogen fuel cells electrocatalysis, catalytic reactions involving hydrogen, etc. [1-4].

In the 1980s, Haruta discovered a low-temperature catalytic oxidation reaction using nano-Au catalysts. Since this discovery, Au catalysis has gained attention from researchers [5]. The electronic configuration of gold (0), gold (I), and gold (-I) anions is  $5d^{10}6s^1$ ,  $5d^{10}6s^0$  and  $5d^{10}6s^2$ , respectively. Therefore, Au is a metal that can be considered as an effective catalyst. It is also regarded as an appealing catalytic metal because the size of its particles can be minimized to nanoscale resulting in an increase in the amount of catalytic active sites, thus improving catalytic performance for oxidation, hydrogenation, etc. [6-8]. Au is not a suitable catalyst for hydrogenation because of its minimal ability to activate  $H_2$ . To improve the catalytic performance (e.g., activity, selectivity and lifetime) of monometallic Au nanocatalysts, they are usually alloyed with a secondary metal used in chemical industries. In recent years, Au has been coupled with more active metals such as miscible metals like Pd, Cu, and Ag as well as only partially miscible or even immiscible metals like Ni, Ru, Pt, Co, and Fe [9-12]. Bimetallic nanosystems may create a synergistic catalytic effect that involves the ligand and strain effect. The ligand effect occurs as a result of hetero-atom bonds and the strain effect is the outcome of the different average metal-metal bond lengths. The ligand and strain effect modify the electronic structure of bimetallic systems by changing their electronic environment and the orbital overlap, respectively. Consequently, the synergistic catalytic effects created through alloying with Au typically results in a number of catalytic functions for applications in clean energy and environmental issues. The modified bimetallic Au-Cu catalysts were summarized by Hutchings et al. [13]. Also, the bimetallic Au-Pd and Au-Pt catalysts were summarized by Ouyang et al. [14]. Our previous study [15] showed that the atomic oxygen adsorption energy for Au@Cu (100) and Au@Pt(100) was stronger in comparison with Au (100). We also found that the atomic oxygen adsorption energy was sensitive to

surface coverage; at a low coverage ( $\theta < 0.5$ ), the binding of oxygen was the strongest on the Au-Cu (100) surface. However, as the coverage increased ( $\theta > 0.5$ ), the binding of oxygen on the Au-Pt (100) became the strongest. In continuation of our previous studies [15,16], we utilized the changes in the hydrogen binding energy to determine the hydrogenation activity of Au (100), Pt (100), and Cu (100) as well as those of the bimetallic Au@Cu (100) and Au@Pt (100) surfaces. To study the interaction between hydrogen and metallic surfaces, the evaluation of the dependence of the hydrogen adsorption states on both the metal surface composition and the exposure to hydrogen is of importance. There are few *ab initio* studies regarding these features. In their study of the atomic H, N, O, and S adsorption on Pt@Au bimetallic surface overlayers, Chen et al. [17] utilized density functional theory (DFT) calculations. It was found that bimetallic systems showed a qualitatively different behavior for trends in binding energy. In another study, Juarez et al. [18] studied the hydrogen interaction with Au modified by Pd and Rh using DFT. They showed that the reactivity of the gold surface in bimetallic systems can be tuned by varying the hydrogen coverage. Taking these studies into account, we examined the adsorption of hydrogen atoms on the Au (100), Pt (100), Cu (100), Au@Cu (100), and Au@Pt (100) surfaces. In addition, the dependence of hydrogen adsorption on their surface coverage was illustrated.

---

## 2. Computational methods

First-principle calculations based on spin-polarized DFT were carried out using the Quantum Espresso v4.3.2 [19], which is a code based on the generalized gradient approximation density-functional theory (DFT). The code provides an iterative solution of the Kohn-Sham equation for a system with periodic boundary conditions using the plane-wave basis set. To represent the electron-ion core interaction, it employs the projected augmented wave (PAW) approach [20]. The exchange-correlation potentials are described by

the generalized gradient approximation of Perdew et al., known as PW91 [21]. In all cases, the energy cutoff for the plane waves was set to 50 Ry ( $\sim 680.2$  eV), thus assuring a good convergence in energy. The  $3 \times 3 \times 1$  Monkhorst–Pack [22] mesh, as the optimum grid, was used in sampling the Brillouin zone. All systems were modeled using a slab that contained five atomic layers of metal (100) (Au, Cu, and Pt) containing 40 atoms, separated by a vacuum space equivalent to eight layers. In this way, there were no interactions between the adsorbed intermediates and the bottom surface of the next slab. All the metal layers were allowed to relax using the Hellman–Feynman forces computed at each geometry step. The pseudomorphic bimetallic structures, Au@Cu and Au@Pt, were built by replacing the topmost layer of the Au (100) slabs with a layer of the corresponding metals (Cu and Pt). The Eads of atomic hydrogen on metallic surfaces are given by

$$E_{\text{ads}} = -1/n_{\text{H}} [E_{\text{slab}+n_{\text{H}}} - (E_{\text{slab}} + n_{\text{H}}E_{\text{H}})] \quad (1)$$

Where  $E_{\text{slab}+n_{\text{H}}}$ ,  $E_{\text{slab}}$ , and  $E_{\text{H}}$  are the total energy of the hydrogen adsorption system, a pure relaxed surface, and a hydrogen atom, respectively.  $n_{\text{H}}$  is the number of adsorbed hydrogen atoms on the surface of the unit cell. The charge analysis was done by Löwdin population analysis based on the projected electron densities of states (PDOS).

### 3. Results

#### 3.1. Electronic and Magnetic Properties of Pure Au (100), Pt (100), Cu (100), Au@Cu (100), and Au@Pt (100) surfaces

According to the d-band theory of Hammer and Nørskov [23], adsorption energies can be related to the d-band position. In this model, the position of the d-states contributing to the interaction is displayed with the center of the d-band, which is a single d-state at  $E_{\text{d}}$ . In this section, the electronic and magnetic properties of the optimized pure slabs, i.e., slabs without chemisorbed hydrogen, are discussed in detail. The monometallic Au (100), Pt (100), and Cu (100) along with the bimetallic Au@Cu (100) and Au@Pt (100) surfaces examined in this paper are shown in Fig. 1. The monometallic slab is composed of five metal layers. The bimetallic pseudomorphic surfaces are composed of five metal layers with Pt or Cu in the first layer and Au in the other four. The lowermost metal layer in a periodic slab calculation is symmetrically identical to the topmost layer. As a result, the complete structural relaxation of the slab leads to identical relaxations for the top and bottom layers. The location of the d-band center in relation to the Fermi level was utilized to analyze the chemisorption of adsorbates on metal surfaces.

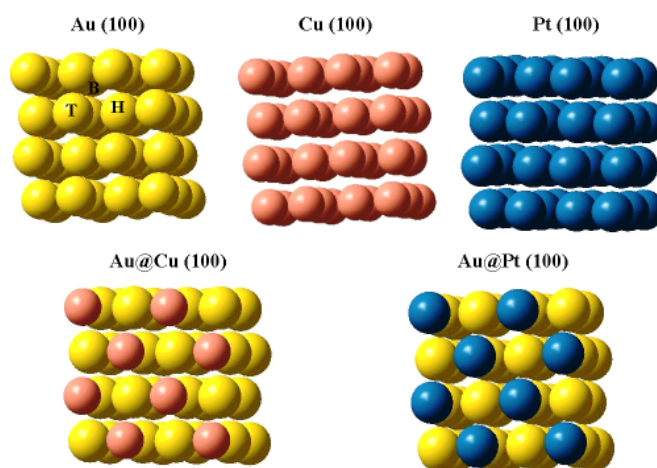


Fig. 1. Side view of five-layered monometallic Au (100), Cu (100), and Pt (100) and bimetallic Au@Cu (100) and Au@Pt (100) slabs. Hollow adsorption site (H), Bridge site (B), and Top site (T).

This parameter determined the amount of interaction between the adsorbate orbital states and metal d states for electron donation and backdonation [24]. The d-band center is defined as the first order moment of the normalized projected density of states about the Fermi level. The various moments of the DOS for one specific orbital or the total sum of orbitals are determined using:

$$\mu_n = \frac{\int_{-\infty}^{+\infty} \varepsilon^n \rho(\varepsilon - \varepsilon_0) d\varepsilon}{\rho(\varepsilon - \varepsilon_0) d\varepsilon} \quad (2)$$

where  $n$  is the order of the moment,  $\rho$  is the density of states (DOS),  $\varepsilon$  is the energy, and  $\varepsilon_0$  is the reference energy which is usually set to the Fermi energy. The average energy of the DOS, i.e., DOS “band center”, is determined by the first order moment ( $n = 1$ ).

To achieve better insight into the electronic and magnetic properties of pure Au (100), Pt (100), and Cu (100) and pure bimetallic Au@Pt and Au@Cu (100) structures, their total density of states (DOS) and local density of states (LDOS) are plotted in Fig. 2. For all systems, the spin-up and spin-down bands are metallic; therefore, none of them are ferromagnets. In ferromagnetic systems, spin-up bands are semiconducting and spin-down bands are metallic or vice-versa because of ferromagnetic decoupling. For Au (100) and Cu (100), there is no spin polarization, as shown in Figure 2. In these systems, spin-up and spin-down bands are symmetric. A strong upward shift of the d-band center (-1.7eV) in Cu (100) in comparison to Au (100) (-2.1eV) with respect to the Fermi energy leads to stronger adsorption energy due to the larger number of empty anti-bonding states. In Pt (100), Au@Cu (100), and Au@Pt (100) systems, the spin-up and spin-down bands are asymmetric and shift significantly in opposite directions. Therefore, they are spin-polarized; spin paramagnetism is also observed. For this reason, the adsorption energies of the atomic hydrogen obtained from the spin polarized calculation is consider to be a significant effect of spin polarization on adsorption.

### 3.2. Atomic hydrogen adsorption on Au (100), Pt (100), Cu (100), Au@Cu (100), and Au@Pt (100) surfaces

Initially, three adsorption sites (Hollow, Bridge and Top) were examined for all the surfaces. It was found that the most stable adsorption sites for the Au, Pt, and Au@Pt surfaces were bridge sites, while the most stable adsorption site for Cu and Au@Cu surfaces were the hollow sites. The optimized hydrogen-surface vertical distances were 1Å for Au, Pt, and Au@Pt surfaces while these distances were 0.8Å and 1.5Å for Cu and Au@Cu, respectively. There are precedents of atomic hydrogen adsorption studies on Au (100), Cu (100), and Pt (100) surfaces [25, 26, 27, 28]. N’Dollo et al. [27] and G’omez et al. [28] reported the bridge site as the preferential one for H adsorption on the Au (100) surface, and this was in good agreement with our results. Meanwhile, the Au-H vertical distance in this study was 1Å, which agreed well with 0.93Å and 0.89Å reported by N’Dollo et al. and G’omez et al., respectively. In the case of the Pt surface, the bridge site was the most favorable for H adsorption, which was in agreement with our previous studies. The Pt-H vertical distance in our findings was 0.8Å while N’Dollo et al. and G’omez et al. reported it to be 1.06Å and 1.02Å, respectively. Regarding the Cu (100) surface, the most stable site for H adsorption was the hollow site, which was previously reported by Ferrin et al. [25] and G’omez et al. The Cu-H distance at the hollow site was 0.8Å while del V et al. reported it as 0.45Å. Fig. 3 shows that for all the surfaces, the atomic hydrogen adsorption energy decreases with the increase of hydrogen coveragesignifying repulsive interactions between the adsorbed hydrogen atoms at higher coverages. At all the coverages, the value of the adsorption energy for the bimetallic Au@Cu and Au@Pt surfaces was larger than that for the monometallic Au (100), Cu (100), and Pt (100) surfaces; this was in good agreement with the d-band center shift closer to the Fermi energy in bimetallic systems. The Au (100) had the lowest interaction with the atomic hydrogen. The hydrogen adsorption

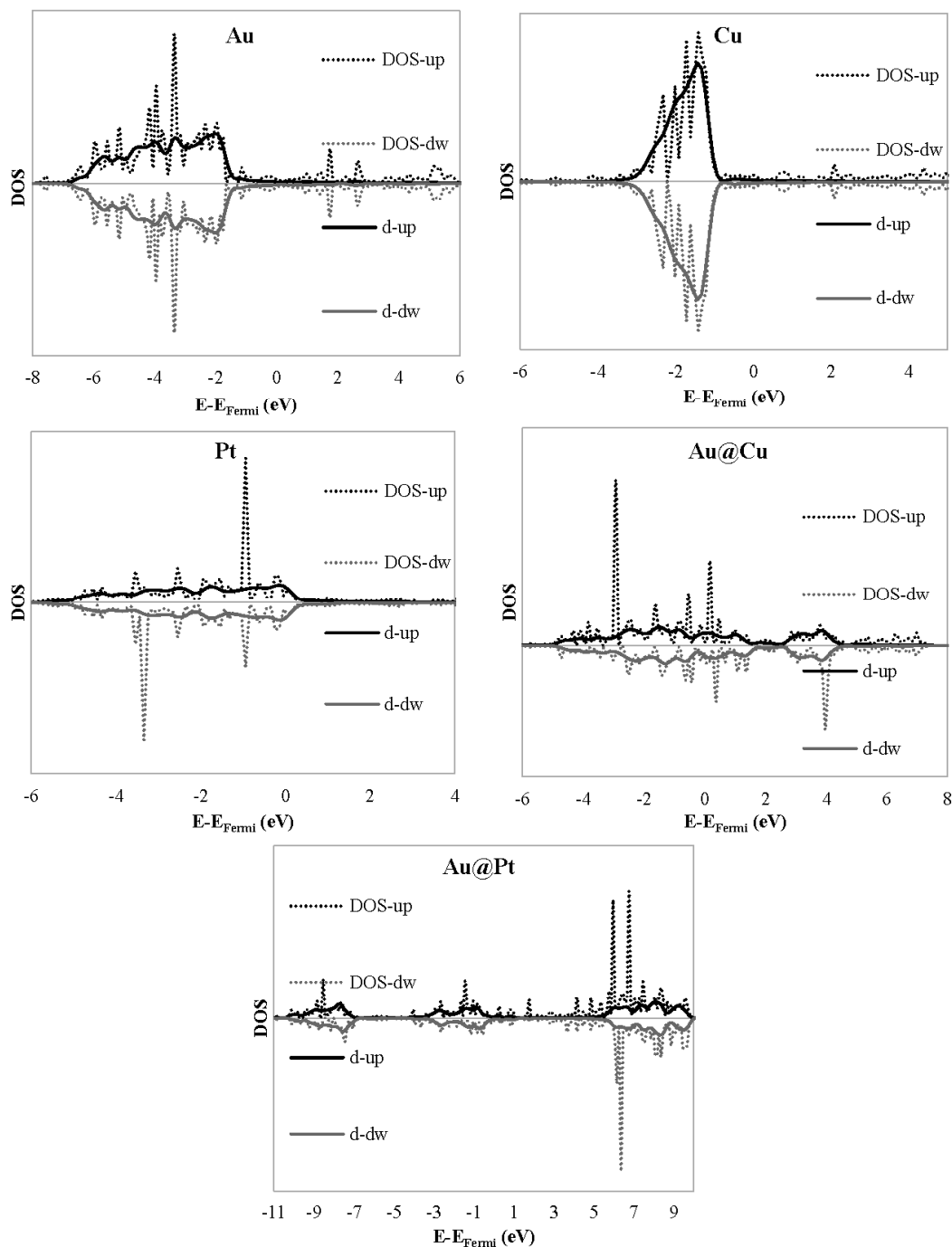


Fig. 2. The total DOS and the DOS projected to d-band of the pure slabs. The Fermi level is the energy zero in all cases.

energies on the Au@Pt (100) surfaces at all coverages were greater than the  $E_b$  of molecular hydrogen. This implied that the dissociative adsorption of a hydrogen molecule was exothermic on this surface. To better understand the atomic hydrogen interaction with different surfaces, the effect of hydrogen adsorption on the projected DOS of the d-band of

the topmost metal layer and second metal layer in the pure slabs are shown in Fig. 4. There was very little disturbance in the electronic DOS for the second metal layers. However, the d-bands for the surface layers of the Cu (100) and Au@Pt (100) systems were changed dramatically by hydrogen adsorption. The projected DOS for hydrogen adsorption on

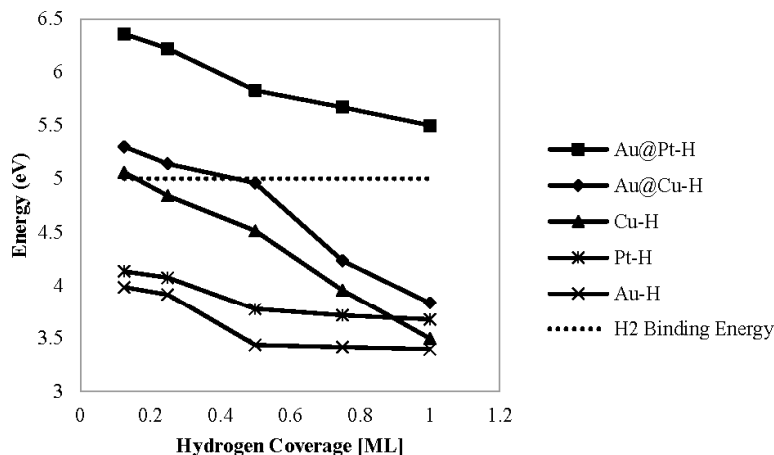


Fig. 3. Hydrogen adsorption energy dependence on hydrogen coverage ( $\theta$ )

monometallic and bimetallic systems at  $\theta = 0.125$  and  $\theta = 0.1$  are shown in Fig. 5. The bonding and antibonding overlaps of the metals d-band with the H-1s state have been determined in  $\theta = 0.125$ . The interaction of the H-1s state with the metal d-band in Au@Cu (100) and Au@Pt (100) was stronger than that of the other surfaces. As a result, the relative location of the bonding state moved nearer to the Fermi level. This stronger interaction caused stronger hydrogen chemisorption energy. The antibonding overlap of the d-band with the H-1s state occurred in unoccupied eigenstates placed above the Fermi level. The differences in the hydrogen atom adsorption on different metallic surfaces were also investigated by the adsorption-induced changes in the Löwdin charges. The Löwdin charge (the number of valence electrons) of each atom in the supercell system was obtained from Löwdin population analysis based on the projected electron densities of states. Table 1 gives the charge changes ( $\Delta Q$ ) for slabs and atomic hydrogen in different supercell systems, which were calculated by subtracting the Löwdin charge of the corresponding component in its isolated form from that in the optimized adsorption structures. A negative value of  $\Delta Q$  implies a gain of electrons by the component. When a hydrogen atom is adsorbed on the metallic surfaces, the hydrogen atom is negatively charged in the Au-H, Cu-H, and Au@Pt-H surfaces, while it is positively charged in the Pt-H and Au@Cu-H. This means that due to the adsorption of the hydrogen atom, Au atoms of Au

(100), Cu atoms of Cu (100), and Pt atoms of Au@Pt (100) surfaces tend to lose the  $6s^1$ ,  $4s^1$ , and  $6s^1$  electrons and reach the electronic configurations of  $5d^{10}$ ,  $3d^{10}$ , and  $5d^9$ , respectively. It should be noted that the presence of gold atoms in the lower layers with  $5d^{10} 6s^1$  configuration can lead to the stability of surface Pt atoms by losing a  $6s^1$  electron and filling the Pt  $5d^9$  orbital. In contrast, the Pt atoms of the Pt (100) surface and the Cu atoms of the Au@Cu (100) surface prefer to gain an electron from hydrogen  $1s^1$  and reach the  $5d^{10} 6s^1$  and  $3d^{10} 4s^2$  electronic configurations. Therefore, it can be concluded that the presence of the second metal plays a fundamental role in the modification of the electronic properties of bimetallic surfaces.

#### 4. Conclusions

The adsorption energies of atomic hydrogen on the (100) surfaces of monometallic Au, Cu, Pt and bimetallic Au@Cu and Au@Pt indicate that the trend of the hydrogen chemisorption on the studied surfaces follows the prediction of the d-band model. According to the total density of states for all the systems, the spin-up and spin-down bands are metallic. Therefore, none of them are ferromagnets. For Au (100) and Cu (100), there is no spin polarization; also, their spin-up and spin-down bands are symmetric. A strong upward shift of the d-band center ( $-1.7\text{eV}$ ) in Cu (100) in comparison to Au (100) ( $-2.1\text{eV}$ ) with respect to the

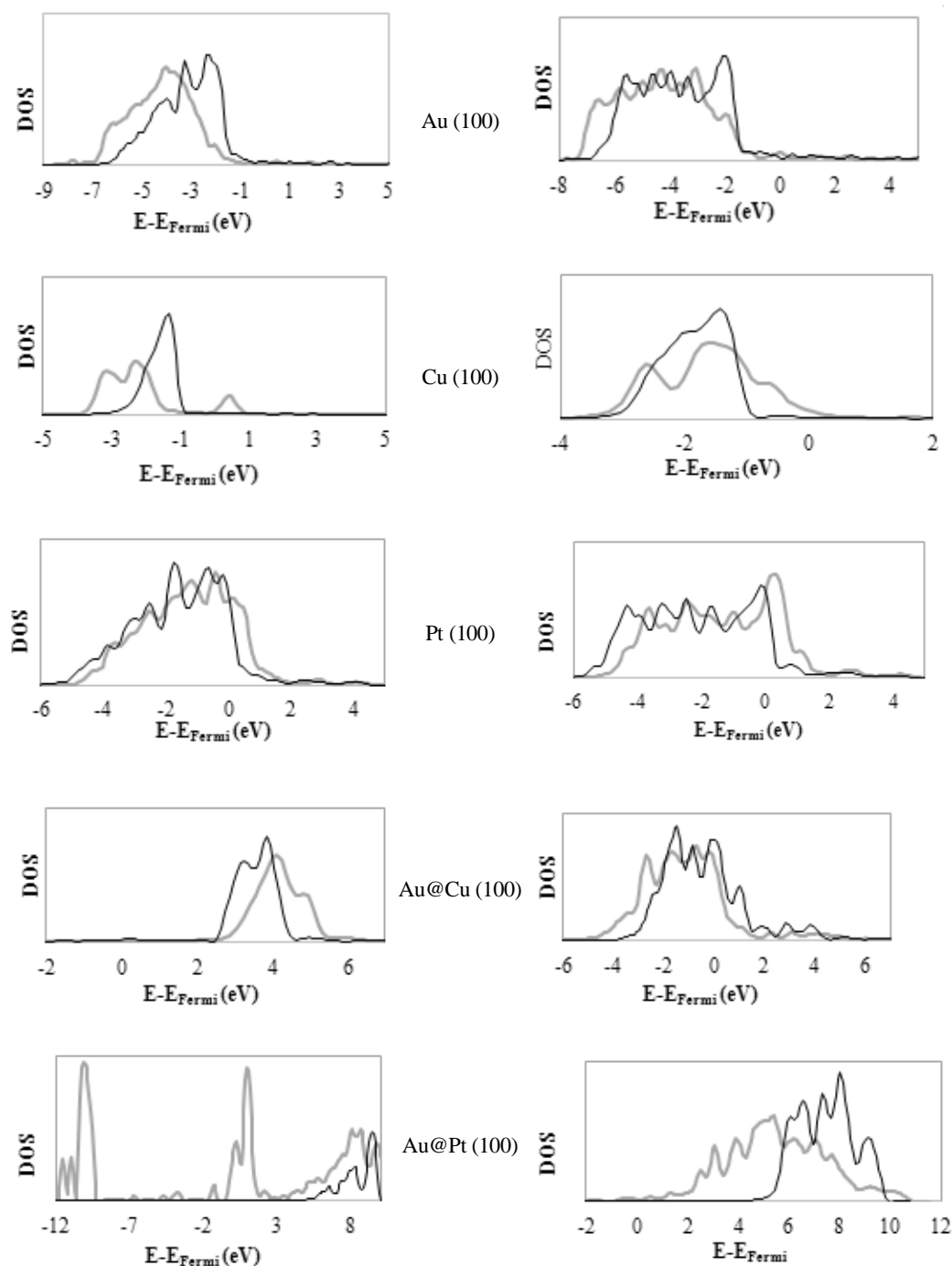


**Fig. 4.** Effect of hydrogen adsorption on projected DOS of d-band in pure slabs. DOS projected to the d-band of pure slab (black lines). DOS projected to the d-band of hydrogen chemisorbed system (gray lines), (left) d-band of topmost layer and (right) d-band of second layer. The Fermi level is the energy zero in all cases.

Fermi energy, leads to stronger adsorption energy due to the larger number of empty anti-bonding states. In Pt (100), Au@Cu (100), and Au@Pt (100) systems, the spin-up and spin-down bands are asymmetric and shift significantly in opposite directions. The energy

differences between the values of hydrogen adsorption energy and  $E_b$  for Au@Cu and Au@Pt surfaces are larger than that the values for Cu, Pt, and Au. This implies that oxygen is scarcely adsorbed on Cu, Pt and Au surfaces.

Table 1. Charge changes of metallic slab and atomic hydrogen in different systems

		$\Delta Q$
Au-H	Au slab	+0.690
	Atomic Hydrogen	-0.493
Cu-H	Cu slab	+0.187
	Atomic Hydrogen	-0.083
Pt-H	Pt slab	-0.498
	Atomic Hydrogen	+0.159
Au@Cu-H	Au@Cu slab	-0.109
	Atomic Hydrogen	+0.073
Au@Pt-H	Au@Pt slab	+0.341
	Atomic Hydrogen	-0.492

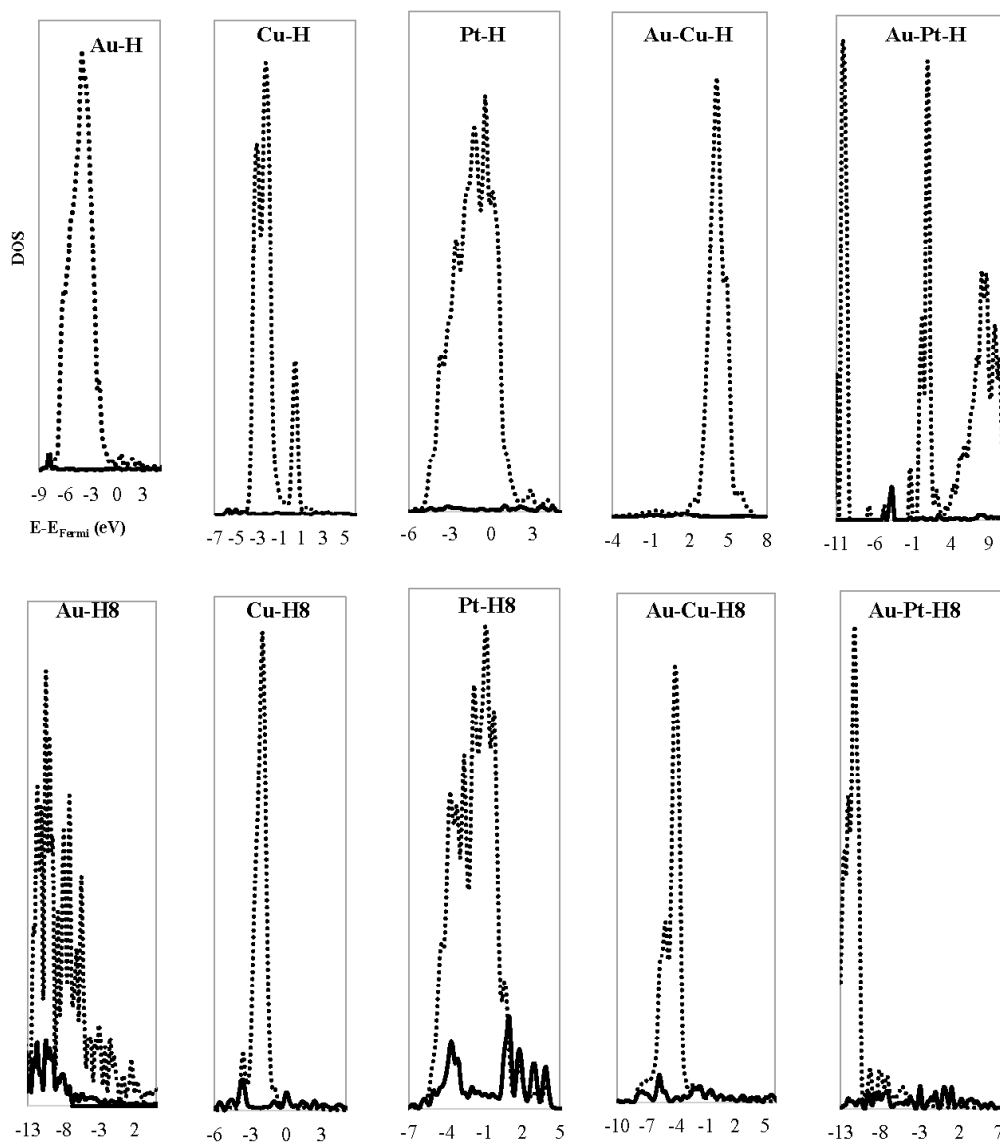


Fig. 5. Projected DOS for hydrogen adsorption on different systems at  $\theta = 0.125$  (one H atom) and  $\theta = 1$  (eight H atoms). DOS projected to surface metal d-band (solid lines). DOS projected to the H-1s state (dotted lines). The Fermi level is the energy zero in all cases.

## References

- [1] Ferrin P. Kandoia S. Udaykumar Nilekara A. and Mavrikakisa M., "Hydrogen absorption and diffusion on and in transition metal surfaces: A DFT study", *Surf Sci*, 2012, 606:7.
- [2] Edwards P. P. Kuznetsov V. L. David W. I. F. and Brandon N. P., "Hydrogen and fuel cells: Towards a sustainable energy future", *Energy Policy*, 2008, 36:4356.
- [3] Neef H. J., "International overview of hydrogen and fuel cell research", *Energy*, 2009, 34: 327.
- [4] Gupta R. B., 1<sup>st</sup> ed., *Hydrogen Fuel: Production, Transport and Storage*, CRC Press, 2009.
- [5] Haruta M., "When Gold Is Not Noble: Catalysis by Nanoparticles", *Chem Rec*, 2003, 3: 75.
- [6] Ma Z. Dai S., "Design of Novel Structured Gold Nanocatalysts", *ACS Catal*, 2011, 1: 805.
- [7] Ma Z. Dai S., "Development of novel supported gold catalysts: A materials perspective", *Nano Res*, 2011, 4:3.
- [8] Gawande M. B. Rathi A. K. Tucek J. Safarova K. Bundaleski N. Teodoro O. M. N. D. Kvitek L. Varma R. S. and Zboril R., "Magnetic gold nanocatalyst (nanocat-Fe-Au): catalytic applications for the oxidative esterification and hydrogen transfer reactions", *Green Chem*, 2014, 16:4137.
- [9] Lucci F. R. Darby M. T. Mattera M. F. G. Ivimey C. J. Therrien A. J. Michaelides A. Stamatakis M. Charles E. and Sykes H., "Controlling Hydrogen Activation, Spillover, and Desorption with Pd-Au Single-Atom Alloys", *J Phys Chem Lett*, 2016, 7:480.
- [10] Kim K. J. and Ahn H. G., "Bimetallic Pt-Au Nanocatalysts on ZnO/Al<sub>2</sub>O<sub>3</sub>/Monolith for Air Pollution Control", *J Nanosci Nanotechnol*, 2015, 15:6108.
- [11] Babu S. G. Gopiraman M. Deng D., Wei K. Karvembu R. and Kim I. S., "Robust Au-Ag/graphene bimetallic nanocatalyst for multifunctional activity with high synergism", *Chem Eng J*, 2016, 300:146.
- [12] Calzada L. A. Collins S. E. Han C. W. Ortolan V. and Zanella R., "Synergetic Effect of Bimetallic Au-Ru/TiO<sub>2</sub> Catalysts for Complete Oxidation of Methanol", *Appl Catal B*, 2017, 207: 79.
- [13] Hashmi A. S. K. and Hutchings G. J., "Gold catalysis", *Angew Chem Int Ed*, 2006, 45:7896.
- [14] Ouyang R. and Li W. X., "First-principles study of the adsorption of Au atoms and Au<sub>2</sub> and Au<sub>4</sub> clusters on FeO/Pt (111)", *Phys Rev B*, 2011, 84:165403.
- [15] Jalili S. Zeini Isfahani A. and Habibpour R., "Atomic oxygen adsorption on Au (100) and bimetallic Au/M (M = Pt and Cu) surfaces", *Comput Theor Chem*, 2012, 989:18.
- [16] Jalili S. Zeini Isfahani A. and Habibpour R., "DFT investigations on the interaction of oxygen reduction reaction intermediates with Au (100) and bimetallic Au/M (100) (M = Pt, Cu, and Fe) surfaces", *International Journal of Industrial Chemistry*, 2013, 4:33.
- [17] Chen W. Schneider W. F. and Wolverton C., "Trends in atomic adsorption on Pt<sub>3</sub>M(111) transition metal bimetallic surface overlayers", *J Phys Chem C*, 2014, 118:8342.
- [18] Juarez F. Soldano G. Santos E. Guesmi H. Tielens F. and Mineva T., "Interaction of Hydrogen with Au Modified by Pd and Rh in View of Electrochemical Applications", *Computation*, 2016, 4:26.
- [19] Giannozzi P. Baroni S. Bonini N. Calandra M. Car R. Cavazzoni C. Ceresoli D. Chiarotti G. L. Cococcioni M. Dabo I. Dal Corso A. Fabris S. Fratesi G. de Gironcoli S. Gebauer R. Gerstmann U. Gougoussis C. Kokalj A. Lazzeri M. Martin-Samos L. Marzari N. Mauri F. Mazzarello R. Paolini S. Pasquarello A. Paulatto L. Sbraccia C. Scandolo S. Sclauzero G. Seitsonen A. P. Smogunov A. Umari P. Wentzcovitch R. M., "QUANTUM ESPRESSO: a modular and open-source software project for quantum simulations of materials", *J Phys :Condens Matter*, 2009 21:395502.

[20] Blöchl P. E., "Projector augmented-wave method", Phys Rev B., 1994 50:17953.

[21] Perdew J. P. and Wang Y., "Accurate and simple analytic representation of the electron-gas correlation energy", Phys Rev B., 1992 45:13244.

[22] Monkhorst H. J. and Pack J. D., "Special points for Brillouin-zone integrations", Phys Rev B., 1976 13:5188.

[23] Hammer B. and Nørskov J. K., "Electronic factors determining the reactivity of metal surfaces", Surf Sci., 1995, 343:211.

[24] Hammer B. Morikawa Y. and Norskov J. K., "CO chemisorption at metal surfaces and overlayers", Phys Rev Lett., 1996, 76:214.

[25] Ferrin P. Kandoia S. Udaykumar Nilekara A. and Mavrikakisa M., "Hydrogen adsorption, absorption and diffusion on and in transition metal surfaces: A DFT study", Surf Sci., 2012, 606:679.

[26] Pang X. Y. Xue L. Q. and Wang G. C., "Adsorption of Atoms on Cu Surfaces: A Density Functional Theory Study", Langmuir, 2007, 23:4910.

[27] Ndollo M. Moussounda P. S. Dintzer T. and Garin F., "A Density Functional Theory Study of Methoxy and Atomic Hydrogen Chemisorption on Au(100) Surface. J Mod Phys, 2013, 4:409.

[28] Gómez E. D. V. Amaya-Roncancio S. Avalle L. B. Linares D. H. and Gimenez M. C., "DFT Study of Adsorption and Diffusion of Atomic Hydrogen on Metal Surfaces", appl surf sci, 2017, 420:1.